Research Article

Sherin A. Saraireh*, Mohammednoor Altarawneh*, and Mouad A. Tarawneh

Nanosystem's density functional theory study of the chlorine adsorption on the Fe(100) surface

https://doi.org/10.1515/ntrev-2021-0051
received April 27, 2021; accepted July 15, 2021

Abstract: This contribution investigates chlorine (Cl) interaction with the Fe(100) surface, with a focus on governing adsorption energies and geometrical features at the nanoscale using the density functional theory (DFT) approach. The Cl/Fe(100) system can be considered as a building block to create nanosystems with specific and desired electronic, material, mechanical, or environmental properties. We report adsorption energies, surface relaxations. and buckling distances for Cl adsorbed as a function of Cl coverage. The computational DFT framework employs a vdW-DF functional with coverages varying from 0.25 to 1 ML. Adsorption at a bridge site with coverage of 0.5 ML appears to be the most preferred site, with an adsorption energy of −4.44 eV. For all coverages, Cl adsorption at the bridge and hollow sites incurs slightly higher adsorption energies than adsorption at the top (T) site. The potential energy surface (PES) for the dissociation of a Cl molecule over the Fe(100) surface was calculated. Dissociative adsorption of the Cl molecule on Fe(100) ensues *via* a modest activation barrier of only 0.58 eV in a noticeably exothermic reaction of 2.94 eV. In agreement with experimental observations, the work function decreases upon Cl addition in reference to the clean iron surface. The electronic interaction between Cl and the Fe(100) surface was examined by calculating the differential charge density distribution of the most stable structure (B-0.5 ML). The vdW-DF interactions increase the adsorption energies and reduce the equilibrium distances when compared with the corresponding results from plain DFT.

Keywords: iron surfaces, chlorine, DFT calculations, vdW-DF functional, nanosystem

1 Introduction

The profound chemical reactivity of iron surfaces with chlorine species is of prime importance for several environmental and industrial concerns, including chlorination of aromatic pollutants (most notably notorious dioxins) and corrosion of equipment [1–3]. For instance, the system of halogens–iron plays a central role in deriving the halogenation cycle of aromatic compounds in scenarios pertinent to municipal waste incineration and recycling of electronic wastes [4]. From a safety perspective, the interaction of iron and chlorine has been extensively studied to comprehend chemical phenomena that prevail under corrosive HCl environments [5] and chlorine-containing salts (*i.e.*, seawater) [6]. Chlorine chemisorption on the low-index (100) and (110) iron surfaces have been investigated on the basis of many aspects [7–9]. Dowbin and Jones [1] investigated the adsorption of Cl_2 on the Fe(100) surface using Auger electron spectroscopy (AES) and low energy electron diffraction (LEED) approaches at room temperature. They illustrated that the change in the work function is proportional to the chlorine coverage, with a maximum value of 1.43 eV at complete saturation. Chlorine adsorption over a four-fold site (hollow site) is more stable than that at other sites. Upon heating, chlorine either desorbs into the vacuum or undergoes bulk diffusion. Along the same line of enquiry, Hino and Lambert [2] studied the interaction of chlorine with the Fe(100) surface at low pressure using Auger spectroscopy, thermal desorption, X-ray and ultraviolet photoemission spectroscopy (XPS and UPS) techniques. They demonstrated that the first adsorbate layer comprises $FeCl_2$ rather than FeCl or non-dissociated chlorine molecules. After the complete formation of a chemisorbed overlayer and at 300 K, the growth of the iron chloride layer is sustained.

* **Corresponding author: Sherin A. Saraireh,** Department of Physics, College of Science, Al-Hussein Bin Talal University, P.O. Box 20, Ma'an, Jordan; Physics Department, Faculty of Sciences, Taibah University, Al-Madeina Al-Munawarah, Saudi Arabia, e-mail: sherin_saraireh@ahu.edu.jo
* **Corresponding author: Mohammednoor Altarawneh,** Department of Chemical and Petroleum Engineering, United Arab Emirates University, Sheikh Khalifa Bin Zayed Street, Al-Ain, 15551, United Arab Emirates, e-mail: mn.altarawneh@uaeu.ac.ae
Mouad A. Tarawneh: Department of Physics, College of Science, Al-Hussein Bin Talal University, P.O. Box 20, Ma'an, Jordan

Computationally, several density functional theory (DFT) studies have provided atomic-based insights into the Cl/Fe configurations with a focus on governing electronic/structural properties and thermodynamic stability at different chlorine coverages [3,7–9]. The binding, structures, and reactions of Cl, Cl_2, HCl, and HCl + O with the Fe(100) structure were investigated based on atom superposition and electron delocalization (ASED) molecular orbital theory [3]. Cl_2 was found to readily dissociate over one-fold and two-fold sites [3]. Previous theoretical calculations provided mechanistic insight into the growth of the $FeCl_2$ phase *via* the continuous adsorption of Cl atoms over the Fe(100) surface using generalized gradient approximation-projector augmented wave (GGA-PAW) [9] but without providing an intrinsic reaction barrier. At a 0.75 ML coverage, the four-fold (hollow) and two-fold (bridge) sites were found to be slightly more preferred than the top sites, with adsorption energies of −3.50, −3.39 and −3.29 eV, respectively. Nonetheless, the marginal difference in energies among the former values most likely resides within the accuracy benchmark of the adapted DFT calculations. Our comprehensive DFT study [9] on the interaction of atomic chlorine over the Fe(100) surface presented binding chemisorption energies for on-surface and substitutional adsorption of chlorine using a plain DFT functional. A thermodynamic stability diagram was constructed over a wide range of chlorine chemical potentials to simulate real operational conditions encountered in iron corrosion by chlorine. Nonetheless, our previous study deployed a standard DFT functional without accounting for the long-term interactions that may result from van der Waals (vdW) forces.

To this end, this contribution reports values for adsorption energies, equilibrium geometries, and differential charge density distributions pertinent to the Cl/Fe(100) system. Furthermore, activation energies and work functions are calculated. Computed binding energies take into account the contribution from long-term interactions [10] using the van der Waals correction functional (vdE–DF) [11,12], which has been accounted for *via* the inclusion of a dispersion correction function (DFT-D). An important goal of the current study is to provide underlying kinetic parameters for the uptake of chlorine molecules by the Fe(100) surface. Such information is vital to attain a detailed understanding of processes that dictates the chlorination of iron into its chloride forms. Likewise, the acquired thermodynamic values are expected to enable the construction of stability phase diagrams of Fe–Cl phases at practical conditions germane to varying values of chlorine chemical potential.

2 Methodology

We carry out all computations using spin-polarized density functional theory (DFT) calculations. The PAW-GGA method of PW91 is used in all spin-polarized calculations [13–15] as implemented in the Vienna *ab initio* simulation (VASP) package [16,17]. The van der Waals correction functional (vdE–DF) by Dion *et al.* [11] refines adsorption energies taking into account the effect of long-range interactions. The calculations consider the ferromagnetism character of Fe atoms in which the magnetic moment of partially filled Fe sites rests at $\pm 5.0\,\mu$B [18].

The Fe(100) surface was modeled using a supercell with six layers. To identify the most favorable sites, the bottom two layers were kept fixed at their bulk positions with the first four layers, and the adsorbate atoms were allowed to relax during the optimization. A sampling of the irreducible part of the Brillouin zone was carried out based on automatic generation of κ-points based on a Monkhost-Pack mesh of $(3 \times 3 \times 1)$ [19]. In the z direction, a vacuum spacing of 15 Å separates images along the z-direction in which a dipole correction is imposed. The kinetic energy cutoff was set at 400 eV. Optimizing one structure with eight atomic layers (H-0.25) at 500 eV cutoff energy and $4 \times 4 \times 1$ κ-points sampling has changed its associated adsorption energy marginally within 2.6%.

Relaxations ($\nabla_{ab}\%$) between layers a and b are calculated based on the d spacing in the bulk, d_i, with respect to the spacing on the surface d_{ab}:

$$\nabla_{ab}\% = \frac{d_{ab} - d_i}{d_i} \times 100\%. \tag{1}$$

The adsorption energy ($E_{ads.}$) and the chemisorption energy (E_C) are computed based on

$$E_{ads.} = \frac{1}{n}[E_{Cl+surface} - (nE_{Cl} + E_{surface})], \tag{2}$$

$$E_C = \frac{1}{n}\left[E_{Cl+surface} - \left(\frac{n}{2}E_{Cl_2} + E_{surface}\right)\right], \tag{3}$$

where $E_{Cl+surface}$ represents the total energy of the optimized surface with atomic Cl adsorbed, n stands for the number of adsorbed Cl atoms, E_{Cl} is the single Cl atom's ground state energy, $E_{surface}$ is the total energy of the clean surface without adsorption of the Cl atoms, and E_{Cl_2} denotes the gas-phase Cl_2 molecule's ground state energy.

Charge transfer was examined by calculating the differential charge density:

$$\Delta\rho = \rho_{Cl+surface} - \rho_{clean\ surface} - \rho_{n(Cl)}, \tag{4}$$

where $\rho_{Cl+surface}$, $\rho_{clean\ surface}$ and $\rho_{n(Cl)}$ denote the charge distributions for the optimized structure of the relaxed surface with the adsorbate, the free Cl surface, and the Cl adsorbate fixed in their adsorption geometries, respectively. Bader's formalism [20] provides partial charges for selected structures. Activation energies were estimated based on the climbing image nudged elastic band (CI-NEB) method [21]. This approach locates the minimum energy structure of the transition state by surveying the potential energy surface that consists of five images between the reactants and products.

3 Results and discussion

3.1 Fe(100) clean surface

The calculated lattice constant for the bulk Fe is 2.828 Å. This value was obtained by minimizing energy with respect to the volume of the unit cell. This value appears in very good agreement with previous experimental measurements of 2.845 Å [22] and other theoretically calculated values of 2.828 Å [9], 2.830 Å [23], and 2.834 Å [24]. The derived value of the bulk interlayer spacing (d_o) is 1.1 Å. The calculated relaxations between the first and second layers as well as second and third layers for the Fe(100) surface with analogous literature values are listed in Table 1. For the Fe(100) surface, the spacing between the first and second layers is lower than the bulk interlayer spacing (d_{12} = −4.15%). This effect is compensated by an expansion between the second and third layers (d_{23} = +2.65%). Bearing in mind the accuracy margin of the experimental measurements (*i.e.*, ±3), computed values of d_{12} and d_{23} are in relative accord with literature values [9,25–27].

Table 1: Comparison between values of relaxation computed herein and corresponding literature values

Relaxation	Refs. [9,25–27]		Current calculations
	Experimental values	Other theoretical values	
∇_{12} (%)	−1.40 ± 3	−3, −3.50	−4.15
∇_{23} (%)	5.0 ± 2	1.7, 2.30	2.65

∇_{ab} (%) refers to the relative difference in spacing between the bulk and the two adjacent layers a and b (as calculated from equation (1)).

As shown in Figure 1(a), the Fe(100) surface displays three distinct adsorption sites on top of one of the Fe atoms (one-fold, T), a bridge between two surface Fe atoms (two-fold, B), and at a hollow between four surface Fe atoms (four-fold, H).

3.2 Cl adsorbed on the Fe(100) surface

Different Cl/Fe(100) configurations at coverages varying from 0.25 to 1 ML are studied. Adsorption and chemisorption energies and some important geometrical features for all configurations are presented in Table 2. For all coverages, adsorption at two-fold (B) and four-fold (H) adsorption sites is more favored than adsorption at the one-fold (T) sites. At 0.5 ML coverage, B and H sites are found to be more preferred than T sites with adsorption energies (chemisorption energy) of −4.44 (−3.00), −4.39 (−2.97), and −4.06 (−2.62) eV, respectively. For all sites, 0.5 ML coverage is shown to be the most stable configuration among the same site based on the values of adsorption and chemisorption energies. Overall, B site with coverage of 0.5 ML appears to be the most preferred site with chemisorption energy of −3.0 eV. At this site, the average Cl–Fe bond length is 2.31 Å, and the metal–adsorbate distance is 1.84 Å.

At the 0.75 ML coverage, the four-fold site (H) is found to be more preferred than the bridge (B) and top (T) sites, with adsorption energies of −3.86, −3.65 and −3.64 eV and chemisorption energies of −2.42, −2.21 and −2.20 eV, respectively. The latter results are in very good agreement with the result of Dowbin and Jones [1] and

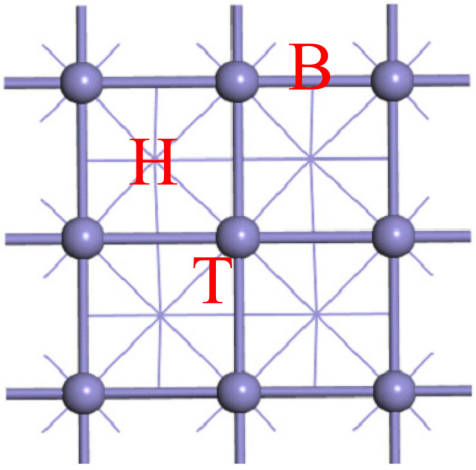

Figure 1: Potential adsorption sites for atomic Cl on the Fe(100) surface. For clarity, atoms in the second layer are denoted by lines.

Table 2: Adsorption energies and structural parameters for Cl/Fe(100)

Site	Coverage Θ (ML)	$E_{ads.}$ (eV)	E_C (eV)	(Cl–Fe) (Å)	R (Å)	H (Å)	(d_{12})%	(d_{23})%
T	0.25	−2.75	−1.31	2.15	2.08	0.11	−1.01	−0.77
	0.5	−4.06	−2.62	2.14	2.16	0.03	5.87	−2.94
	0.75	−3.64	−2.20	2.15	2.30	0.36	−4.93	0.09
	1	−3.08	−1.64	2.10	2.11	0.00	−5.81	−0.78
H	0.25	−3.93	−2.49	2.58	1.45	0.02	7.62	−2.60
	0.5	−4.39	−2.97	2.60	1.65	0.01	9.76	−4.21
	0.75	−3.86	−2.42	2.59	1.48	0.06	5.75	−4.33
B	0.25	−4.38	−2.94	2.34	1.99	0.17	5.65	−2.01
	0.5	−4.44	−3.00	2.31	1.84	0.04	1.27	−4.18
	0.75	−3.65	−2.21	2.30	1.81	0.08	7.27	−2.06
	1	−3.44	−2.00	2.27	1.78	0.01	9.60	−4.57

$E_{ads.}$: adsorption energies, E_C: chemisorption energies, (Cl–Fe): average distance between nearest Fe atoms and Cl atom(s), R: average heights of Cl atoms above the first layers, H: the height between the lowest and highest Fe layers, (d_{12})% relaxation of first and second Fe layers with respect to the clean surface (calculated based on equation (1)), and (d_{23})% relaxation of second and third Fe layers with respect to the clean surface (calculated based on equation (1)).

previous theoretical calculations [9]. The relaxations of the first three Fe layers of the considered surface after adding the adsorbate with respect to the interlayer spacing of the clean surface are presented in Table 2. In all coverages for H and B sites, the presence of chlorine causes an expansion of the first and second interlayer distance and a compression of the second and third interlayer distance. This behavior shows that the first layer of iron relaxes up after interaction with chlorine, while the second layer relaxes down with the attraction of the lower iron atoms. This is in contrast with the case at site T, where each coverage obtained a different behavior. The average Cl–Fe nearest distance (Cl–Fe) increases in the order of T < B < H. The vertical buckling based on the H values in Table 2 in all configurations is very minimal (0.01–0.36) Å, with nearly no buckling observed at full coverages for all sites. The lateral repulsive interactions are expected to play a noticeable role in reducing the binding energy at high coverages [28].

In a corrosive chlorine-containing environment, interactions of chlorine with iron surfaces produce iron chlorides and oxychlorides. Thus, it is of interest to compare distances in Cl–Fe configurations with their corresponding values in bulk iron chlorides. The important geometrical parameters of the most stable configuration B (0.5 ML) are contrasted with analogous distances of bulk $FeCl_2$ and $FeCl_3$ [29], as presented in Table 3. The Cl–Cl distances in the latter structure overshoot their corresponding distances in bulk $FeCl_2$ and $FeCl_3$ by 0.45 and 0.79 Å, respectively. The shortest Fe–Cl spacing in B (0.5 ML) site deviates marginally by 6.5 and 4.9% relative to the analogous values in bulk $FeCl_2$ and $FeCl_3$, respectively.

Table 3: Nearest atomic distances (in Å) for the optimized bulk of $FeCl_2$ and $FeCl_3$ and B (0.5 ML) site

Bond length (Å)	$FeCl_2$ [29]	$FeCl_3$ [29]	B (0.5 ML)
Cl–Cl	3.54	3.20	3.99
Cl–Fe	2.47	2.26	2.31

Despite certain notable differences in some interatomic distances, comparing geometries of B (0.5 ML) with bulk $FeCl_2$ reveals that B (0.5 ML) site retains analogous geometries of bulk $FeCl_2$ to some extent.

Next, we turn our attention to computing activation energies for the dissociation of a chlorine molecule above the surface. Iron readily corrodes in a chlorine-containing environment [30]. This indicates that iron chlorination ensues modest reaction barriers in real scenarios. Figure 2 shows a potential energy surface (PES) for the dissociation of a gas-phase chlorine molecule over the Fe (100) surface. We found the chlorine molecule to be very weakly adsorbed (−0.15 eV, DFT–vdW) while adapting a horizontal-like configuration. This value slightly decreases to −0.10 eV when a plain DFT method is deployed. Rupture of the Cl–Cl bond at two hollow sites demands a modest barrier of only 0.58 eV in a noticeably exothermic reaction of 2.94 eV. The profound surface-mediated effect of the iron surface becomes evident when contrasting the sizable Cl–Cl bond dissociation energy in the gas-phase chlorine molecule at 2.52 eV. The nature of the located transition state as a saddle point was confirmed by evaluating the vibrational frequencies of the structure using the linear response method [31]. The configuration retains one major

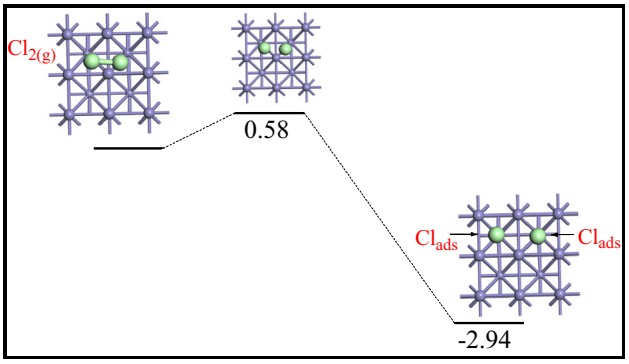

Figure 2: PES for the Fe(100)-assisted fission of a chlorine molecule. Values are in eV in reference to the adsorbed chlorine molecule.

frequency of (258*i*)/cm along with a few other minimal values in the range (34*i*–87*i*)/cm. The latter values most likely correspond to the movements of surface iron atoms.

By considering the surface area of iron surfaces (0.3 m^2/g) and the density of active sites (σ = 2.1 × 10^{-9} mol/cm^2), plots the reaction rate constant (a) and the reaction rate for the dissociative adsorption (b) of a chlorine molecule/over the Fe(100) surface are plotted in Figure 3 according to:

$$k(T) = \frac{s}{\sigma^n}\sqrt{\frac{RT}{2\pi M}}\, e^{-E_a/RT}, \tag{5}$$

where s, M, E_a, and T signify the sticking coefficient (assumed to be 1.0), the molecular weight of Cl_2, activation energy, and temperature, respectively. The calculations of the reaction rate considered a gas-phase concentration at 500 ppm Cl_2 that mimicked mild corrosion conditions. To the best of our knowledge, the literature presents no analogous experimental measurements to compare with computed values herein.

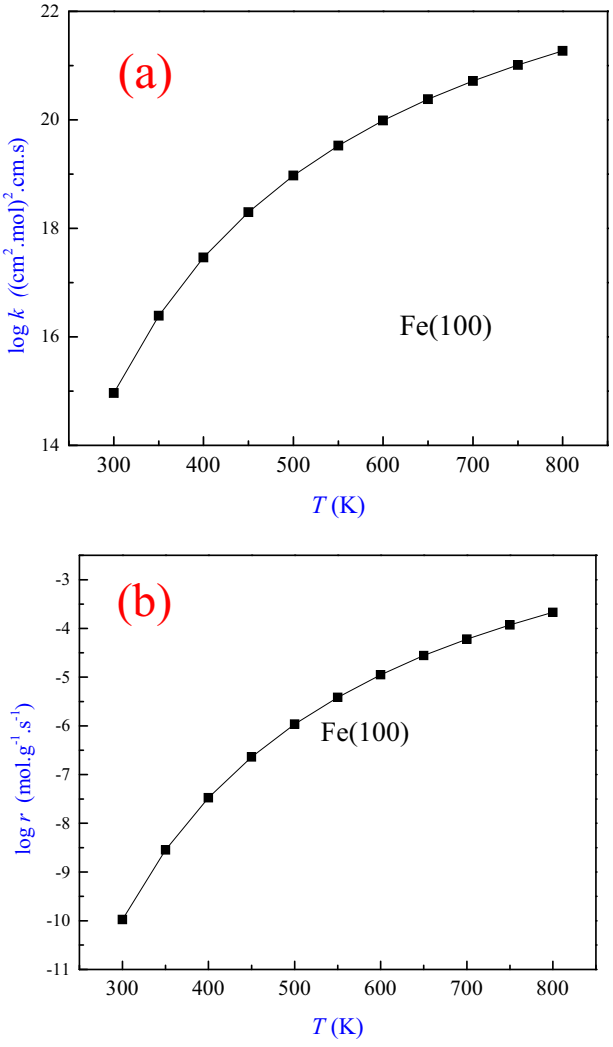

Figure 3: The reaction rate constant (a) and the reaction rate for the dissociative adsorption (b) of a chlorine molecule over the Fe(100) surface.

3.3 Comparison between GGA and van der Waals corrections

The most stable adsorption sites identified above were examined using the GGA-PAW functional. The computed adsorption energies and selected distances are shown in Table 4. The stability ordering of the configurations using GGA-PAW for Cl/Fe(100) configurations is the same as that presented in our previous study [9]. The recalculated GGA-PAW adsorption energies herein depart minimally from our previously computed values [9] in the narrow range of 0.01–0.11 eV. This is due to the number of surface layers of the Fe(100) surface for each study; the current study used six layers, while the previous study used five layers.

For Fe(100) at 0.5 ML, the adsorption energy of the B and H configurations was found to increase by ~0.45 and 0.43 eV, respectively, after the inclusion of van der Waals corrections. For T and B at full coverage, the corresponding adsorption energies increased by ~0.35 and 0.46 eV, respectively. The inclusion of vdW interactions into standard DFT within the GGA brings a large increase in binding for closed-shell species, *i.e.*, singlet-state molecules with surfaces. The enhancement factor, the calculated ratio of the adsorption energy with the inclusion of vdW to the adsorption energy without the inclusion of vdW $\left(\alpha = \frac{E_{ads.(vdW\text{-}DF)}}{E_{asd.(GGA)}}\right)$, herein, marginally departs from units (1.11–1.15) entailing a minor contribution of the

Table 4: Values of $E_{ads.}$ and distance (R) using vdW-DF and GGA-PAW functional for chlorine atom adsorbates on the Fe(100) surface

Site	Surface	vdW-DF		GGA-PAW		α
		$E_{ads.}$(eV)	(R) (Å)	$E_{ads.}$ (eV)	(R) (Å)	
B (0.5 ML)	Cl/Fe(100)	−4.44	1.84	−3.99	1.88	1.11
H (0.5 ML)		−4.39	1.65	−3.96	1.66	1.11
T (1 ML)		−3.08	2.11	−2.73	2.11	1.13
B (1 ML)		−3.44	1.78	−2.98	1.79	1.15

vdW function. This is expected in view of the strong interaction between the distinctly charged Cl and Fe ions. The average height (R) of the Cl atoms above the Fe atoms on the Fe(100) surface calculated using the vdW-DF functional minimally reduces by 0–0.04 Å with respect to that calculated using the GGA-PAW functional [9]. Nonetheless, it is necessary to report values at the vdW-DF level for molecular adsorption systems. In these systems, the two sets of binding energies may significantly differ [32].

Considering the B (0.5 ML) configuration at the Cl/Fe (100) system as an example, the adsorption energy calculated by the vdW-DF functional overshoot calculated by the plain DFT method was a factor of 1.11. This rather small increase in the adsorption energy translates into a negligible difference in the measured height among the two methods at only 0.02%. This finding can now be attributed to the ionic nature of the formed Cl–Fe bonds. Nonlocal interaction increases the adsorption energy on both Fe surfaces and shrinks the equilibrium distance (Table 4). The overlap between the wavefunctions of the iron slab and the Cl atoms accounts for the movement of the electron to higher energy states, and the Cl atoms reach a shorter distance where the magnitude of the attractive force is larger, and the binding energy increases. An inconsistent influence of the inclusion of the vdW function (on geometries and binding energies) with the degree of chlorination most likely originates from the repulsion between electronegatively charged chlorine atoms at high coverages.

3.4 Electronic analysis

The electronic interaction between chlorine and the Fe (100) surface was examined by calculating the differential charge density distribution of the most thermodynamically stable structure (B-0.5 ML). As chlorine adsorbed on the Fe(100) surface, in B (0.5 ML) site, a large degree of charge transfer takes place between Cl atoms and the

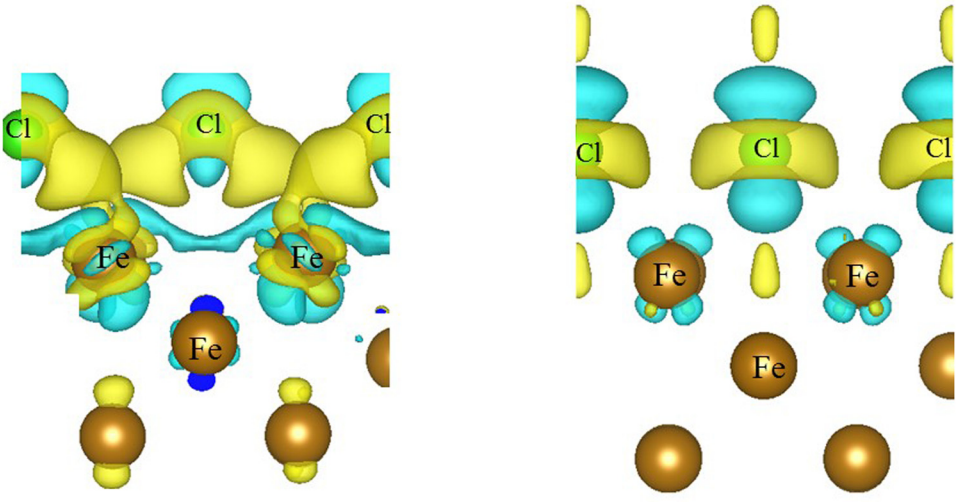

(a) (b)

Figure 4: Charge density difference of Cl adsorbed on the Fe(100) surface in the B (0.5 ML) site. The isosurface was set as 0.005 e/Å^3. The yellow and blue areas represent a gain and a loss in charge, respectively. The brown and light green spheres represent Fe and Cl atoms, respectively. (a) GGA and (b) vdW-DF.

surface Fe atoms using both GGA-PAW and van der Waals correction functions (Figure 4). Charge transfer from the surface to the adsorbate has significantly decreased using the van der Waals correction function in comparison to that obtained using the GGA function. The weak electrostatic interaction and dispersion forces contribute to the adsorption of Cl on the Fe(100) surface. According to the comparison between the above two functions, the charge that accumulates because of the electrostatic effect is larger and extends over a wider domain. Atomic partial charges for selected atoms in the B (0.5 ML) structure are presented in Figure 5. Across most of the investigated configurations, surface iron atoms are reduced by ~0.2 e, while adsorbed chlorine atoms entail a net negative charge of 0.3 e.

The work function (Φ) represents an important electronic fingerprint halogen/iron system. Through combined AES-LEED experiments, Yang *et al.* [33] observed a noticeable change in the work function of Fe(100) and Fe(110) surfaces upon bromine adsorption. The addition of a bromine atom was shown to decrease the work function of the Fe(110) surface while increasing it for Fe(100). The variation in Φ was primarily attributed to a surface charge redistribution that creates an inward pointing dipole. The latter prevails more in the open Fe(100) surface and is sustained by a larger probability of subsurface bromine penetration in reference to the more compact Fe(110) surface. Along the same note of enquiry, the inconsistent change in the work function among halogen (Br/I) –iron configurations prompted Wu and Klepeis [34] to propose a multidipole model in which the change in the work function is governed by the competition between dipoles in different directions. Chen *et al.* [35] illustrated a positive correlation between the changes in vertical dipole moments (with respect to the degree of sulfur coverage above the Fe(100) surface) and that of the work function. Our calculated Φ values for unsubstituted Fe(100) and Fe(110) surfaces amount to 3.92 and 4.09 eV, respectively. These values are in accord with analogous experimental and theoretical values [36–38]. To the best of our knowledge, the literature presents no account of the values of work functions for Cl–iron systems. Figure 6 contrasts Φ values between pure iron surfaces and selected Cl–Fe structures. Dissociation of a chlorine molecule over the Fe(100) surface increases its Φ value by 0.67 eV, while chlorine addition decreases the work function in reference to the pure Fe(110) surface. This trend prevails in bromine addition to the iron surfaces, as in previous studies [34].

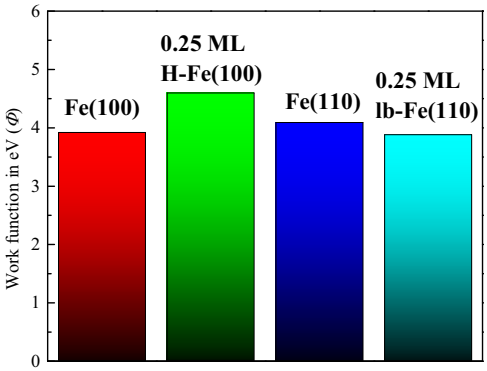

Figure 6: Values of the work function for the Fe(100)/Fe(110) surface and selected Cl–iron structures.

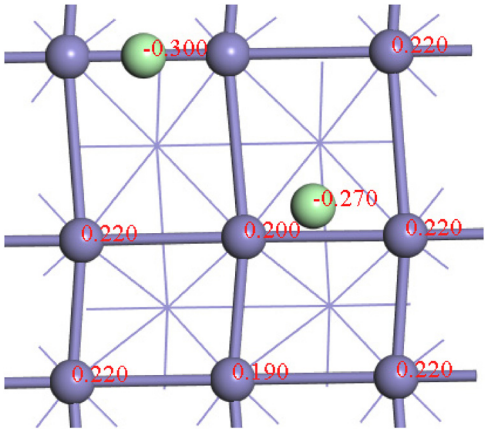

Figure 5: Atomic charges (in e) at selected atoms in the B (0.5 ML) configuration.

4 Conclusions

In this study, DFT–vdW calculations were performed to determine the geometrical features and thermodynamic and kinetic parameters for the adsorption of chlorine on the Fe(100) surface. The obtained activation energy for the dissociative adsorption of the chlorine molecule, along with the density of active sites on the Fe(100) surface, was used to develop a reaction constant and reaction rate for the initial uptake of gaseous chlorine molecules by the Fe(100) surface. As a result of the ionic character of the interaction between chlorine and iron atoms, the enhancement factor characterizing the influence of the vdW functional resides around unity. Chlorine adsorption reduces the work function of the Fe(100) surface. Future research directions may include mapping out the mechanism for the growth of iron chlorides

from the subsurface adsorption of chlorine atoms into the iron bulk.

Acknowledgements: The authors acknowledge access to High Performance Supercomputing facility at the United Arab Emirates University (UAEU).

Funding information: M.A. acknowledges a UPAR grant from the UAEU (grant ID: 21N225).

Author contributions: All authors have accepted responsibility for the entire content of this manuscript and approved its submission.

Conflict of interest: The authors state no conflict of interest.

References

[1] Dowben P, Jones R. Halogen adsorption on Fe(100): I. The adsorption of Cl_2 studied by AES, LEED, work function change and thermal desorption. Surf Sci. 1979;84(2):449–61.
[2] Hino S, Lambert R. Chlorine chemisorption and surface chloride formation on iron: adsorption/desorption and photoelectron spectroscopy. Langmuir. 1986;2(2):147–50.
[3] Li X, Binnemans K. Oxidative dissolution of metals in organic solvents. Chem Rev. 2021;121(8):4506–30.
[4] Altarawneh M, Saeed A, Al-Harahsheh M, Dlugogorski MBZ. Thermal decomposition of brominated flame retardants (BFRs): products and mechanisms. Prog Energ Combust. 2019;70:212–59.
[5] Khaing Aye K, Nguyen TD, Zhang J, Young DJ. Effect of silicon on corrosion of Fe-20Cr and Fe-20Cr-20Ni alloys in wet CO_2 with and without HCl at 650°C. Corros Sci. 2021;179:109096.
[6] Sui J, Lehmusto J, Bergelin MI, Hupa L. Initial oxidation mechanisms of stainless steel Sanicro 28 (35Fe27Cr31Ni) exposed to KCl, NaCl, and K_2CO_3 under dry and humid conditions at 535°C. Corros Sci. 2021;155:29–45.
[7] Pick Š. Comparison of chlorine and oxygen adsorption on the ferromagnetic Fe(001) surface: density-functional theory study. Surf Sci. 2008;602(24):3733–6.
[8] Zhao W, Wang J, Liu F, Chen D. Equilibrium geometric structure and electronic properties of Cl and H2O co-adsorption on Fe(100) surface. Sci Bull. 2009;54(8):1295–301.
[9] Altarawneh M, Saraireh SA. Theoretical insight into chlorine adsorption on the Fe(100) surface. Phys Chem Chem Phys. 2014;16(18):8575.
[10] Kannemann FO, Becke AD. van der Waals interactions in density-functional theory: intermolecular complexes. J Chem Theory Comput. 2010;6(4):1081–8.
[11] Dion M, Rydberg H, Schröder E, Langreth DC, Lundqvist BI. Van der Waals density functional for general geometries. Phys Rev Lett. 2004;92(24):246401.
[12] Berland K, Cooper VR, Lee K, Schröder E, Thonhauser T, Hyldgaard P, et al. van der Waals forces in density functional theory: a review of the vdW-DF method. Rep Prog Phys. 2015;78(6):066501.
[13] Blöchl PE. Projector augmented-wave method. Phys Rev B. 1994;50(24):17953.
[14] Kresse G, Joubert D. From ultrasoft pseudopotentials to the projector augmented-wave method. Phys Rev. 1999;59(3):1758.
[15] Perdew JP, Chevary JA, Vosko SH, Jackson KA, Pederson MR, Singh DJ, et al. Atoms, molecules, solids, and surfaces: applications of the generalized gradient approximation for exchange and correlation. Phys Rev B. 1993;48:4978.
[16] Kresse G, Hafner J. Ab initio molecular dynamics for liquid metals. Phys Rev B. 1993;47(1):558.
[17] Kresse G, Furthmüller J. Efficiency of ab-initio total energy calculations for metals and semiconductors using a plane-wave basis set. Comput Mater Sci. 1996;6(1):15–50.
[18] Lin SY, Tran NTT, Lin MF. Diversified phenomena in metal- and transition-metal-adsorbed graphene nanoribbons. Nanomaterials. 2021;11(3):630.
[19] Monkhorst HJ, Pack JD. Special points for brillouin-zone integrations. Phys Rev B. 1976;13(12):5188.
[20] Tang W, Sanville E, Henkelman GA. grid-based bader analysis algorithm without lattice bias. J Condens Matter Phys. 2009;21(8):084204.
[21] Sheppard D, Terrell R, Henkelman G. Optimization methods for finding minimum energy paths. J Chem Phys. 2008;128(13):134106.
[22] Kittel C, McEuen P. Introduction to solid state physics. New York: Wiley; 2004.
[23] Nguyen TQ, Sato K, Shibutani Y. First-principles study of BCC/FCC phase transition promoted by interstitial carbon in iron. Mater Trans. 2018;59(6):870–5.
[24] Zhong W, Overney G, Toma D. Structural properties of Fe crystals. Phys Rev B. 1993;47(1):95.
[25] Jona F, Legg K, Shih H, Jepsen D, Marcus P. Random occupation of adsorption sites in the c(2 × 2) structure of CO on Fe{001}. Phys Rev Lett. 1978;40(22):1466.
[26] Eder M, Terakura, K, Hafner J. Initial stages of oxidation of (100) and (110) surfaces of iron caused by water. Phys Rev B. 2001;64(11):115426.
[27] Alde M, Mirbt S, Skriver HL, Rosengaard N, Johansson BJ. Surface magnetism in iron, cobalt, and nickel. Phys Rev B. 1992;46(10):6303.
[28] Poberžnik M, Kokalj A. Surprising lateral interactions between negatively charged adatoms on metal surfaces. J Phys Chem Lett. 2020;11(17):7122–6.
[29] Saraireh SA, Altarawneh M. Thermodynamic stability and structures of iron chloride surfaces: a first-principles investigation. J Chem Phys. 2014;141(5):054709.
[30] Cao W. Adsorption of surface active elements on the iron (100) surface, a study based on ab initio calculations. (PhD thesis). Sweden: Royal Institute of Technology; 2009.
[31] Baroni S, Gironcoli Sde, Corso AD, Giannozzi P. Phonons and related crystal properties from density-functional perturbation theory. Rev Mod Phys. 2001;73:515.
[32] Stöhr M, Voorhis TV, Tkatchenko A. Theory and practice of modeling van der Waals interactions in electronic-structure calculation. Chem Soc Rev. 2019;48:4118–54.

[33] Yang Y, Sroubek Z, Yarmoff J. Internal electronic structure of adatoms on Fe(110) and Fe(100) surfaces: a low-energy Li + scattering study. Phys Rev B. 2004;69(4):045420.
[34] Wu CJ, Klepeis JE. Halogen adsorption on transition-metal surfaces: a case study of Cl on Ta(110). Phys Rev B. 1997;55(16):10848.
[35] Chen H, Li B, Wen B, Ye Q, Zhang N. Corrosion resistance of iron-chromium-aluminium steel in eutectic molten salts under thermal cycling conditions. Corros Sci. 2020;173:108798.
[36] Pirug G, Brodén G, Bonzel H. Coadsorption of potassium and oxygen on Fe(110). Surf Sci. 1980;94(2–3):323–38.
[37] Nelson S, Spencer M, Snook I, Yarovsky I. Effect of S contamination on properties of Fe(100) surfaces. Surf Sci. 2005;590(1):63–75.
[38] Ueda K, Shimizu R. LEED-work function studies on Fe (100). Jpn J Appl Phys. 1972;11(6):916.